Polymer Degradation and Stability 97 (2012) 605–614

Contents lists available at SciVerse ScienceDirect

Polymer Degradation and Stability

journal homepage: www.elsevier.com/locate/polydegstab

Using TGA/FTIR TGA/MS and cone calorimetry to understand thermal degradation and flame retardancy mechanism of polycarbonate filled with solid bisphenol A bis(diphenyl phosphate) and montmorillonite

Jie Feng, Jianwei Hao*, Jianxin Du, Rongjie Yang

National Laboratory of Flame Retardant Materials, School of Materials Science and Engineering, Beijing Institute of Technology, 5 South Zhongguancun Street, Haidian District, Beijing 100081, PR China

ARTICLE INFO

Article history:
Received 29 June 2011
Accepted 11 January 2012
Available online 23 January 2012

Keywords:
TGA/FTIR
TGA/MS
Polycarbonate nanocomposite
Aryl phosphate
Flame retardancy

ABSTRACT

Investigation of thermal degradation is essential for understanding flame retardancy mechanism and further tailoring of materials. In this work, polycarbonate was compounded with solid bisphenol A bis(diphenyl phosphate) (S-BDP) and organo-montmorillonite (OMMT) to form a nanocomposite with mainly intercalated and partially exfoliated morphology, and the main flame retardancy activity of the nanocomposite was shown to be in the condensed phase as revealed by cone calorimetry, thermogravimetric analysis coupled with Fourier transform infrared spectrometry (TGA/FTIR) and thermogravimetric analysis coupled with mass spectrometry (TGA/MS). Although the main gaseous pyrolysis products of polycarbonate can't be greatly altered by S-BDP and OMMT, carbonate linkage would be stabilized and vigorous decomposition at higher temperature would be delayed, thereby char residue formation could be promoted. S-BDP also shows slight gaseous phase effect as proved by the detection of phosphorus–oxygen species in TGA/MS. Moreover, the relatively enhanced evolution of PO radicals in the sample filled with only S-BDP suggests that S-BDP alone exhibits a slightly stronger gaseous phase effect than the combination of S-BDP and OMMT. This enhanced condensed phase effect of S-BDP in the presence of OMMT could be associated with the delayed vigorous decomposition at higher temperature due to the barrier effect of OMMT. The peak heat release rate of polycarbonate could not be significantly reduced by substituting S-BDP with OMMT, yet it would prolong the time to peak heat release rate and reduce the smoke toxicity with a smaller release of carbon monoxide. The reduced carbon monoxide release was probably caused by further oxidation of carbon monoxide in the hotter char surface due to the barrier effect of OMMT.

© 2012 Elsevier Ltd. All rights reserved.

1. Introduction

With its high strength, thermal stability and outstanding optical transparency, polycarbonate (PC) is the second large consumed engineering plastic widely used in many areas. Although PC can form char during combustion and is less flammable than many polyolefins, more strict flame retardancy is required under certain circumstances.

Conventional flame retardants used in PC include halogenated, phosphorus-containing, sulfur-containing, siloxane compounds etc. [1–3]. Among these flame retardants, aryl phosphates such as triphenyl phosphate (TPP), resorcinol bis(diphenyl phosphate) (RDP) and bisphenol A bis(diphenyl phosphate) (BDP) are commonly used in PC because of their excellent compatibility with the matrix. During combustion such aromatic phosphates can generate PO radicals to cause flame inhibition in the gaseous phase, as well as promoting char formation in the condensed phase. BDP is an aromatic phosphate with high hydrolytic resistance and it is considered to have slight gaseous effect but mainly to act in the condensed phase [4–6]. Besides conventional flame retardants, nanocomposites technology has been intensively studied recently.

Polymer nanocomposites, as one field of the cutting edge science of nanotechnology, have drawn huge interest from both academia and industry around the world due to their dramatically improved properties [7–12]. Carbon nanotubes [13–17], graphene [18], clays [19–23], polyhedral oligomeric silsesquioxane (POSS) [24–26] and other nano-scaled materials [27–29] have been introduced into PC with the purpose of enhancing various properties. Although polymer nanocomposites exhibit much lower heat release rate than the matrices, usually they fail some protocols such

* Corresponding author. Tel./fax: +86 10 6891 3075.
E-mail address: hjw@bit.edu.cn (J. Hao).

0141-3910/$ – see front matter © 2012 Elsevier Ltd. All rights reserved.
doi:10.1016/j.polymdegradstab.2012.01.011

as UL-94 burning tests. Thus there were some attempts to combine polymer nanocomposites technology and conventional organophosphates to improve the flame retardancy of polymers. Chigwada et al. developed flame retarded polystyrene nanocomposites filled with organo-montmorillonite (OMMT) and several organophosphates [30]. Synergy of flame retardancy between organophosphates and OMMT did occur, and the authors suggested that this methodology could be promisingly extended to other polymeric systems. Pack et al. prepared RDP-coated sodium montmorillonite (RDP MMT-Na^+), and incorporated it into several polymer blends [31]. They found that RDP MMT-Na^+ could not only compatibilize polycarbonate/poly(styrene-co-acrylonitrile) (PC/SAN) blend but also enhance the flame retardancy of the blend. Moreover, the flame retardant effect of RDP MMT-Na^+ was more effective than ammonium-modified clays in this kind of blend.

In our previous work, we employed the melt extrusion method, a method which is favored in industrial manufacturing, to prepare flame retarded polycarbonate nanocomposite filled with solid BDP (S-BDP) and OMMT [32]. S-BDP was more convenient during transportation and processing than the conventional liquid BDP. The PC nanocomposite, with a mainly intercalated and otherwise exfoliated morphology, showed improved flame retardancy highlighted by the synergistic effect of S-BDP and OMMT. Flame retardancy mechanism of this system was primarily explained by the enhanced thermal-oxidative stability of the char residue with the assistance of OMMT. However, whether the thermal degradation of PC would be altered by S-BDP and OMMT is yet unknown.

It is believed that detailed investigation of thermal degradation of a polymer is a rather important issue while dealing with flame retardancy. It could assist us to design or optimize the formulations by understanding the thermal decomposition pathways of the flame retardants and the matrices. Thermal degradation of PC is proposed to have complex reactions including chain scission of isopropylidene linkages, hydrolysis/alcoholysis and Fries rearrangement of carbonate linkages, and cross-linking reaction to form char residue [33–37].

In this work, we first conducted quantitative investigation of combustion behavior of the PC nanocomposite by cone calorimetry. Then, thermogravimetric analysis coupled with Fourier transform infrared spectrometry (TGA/FTIR) and thermogravimetric analysis coupled with mass spectrometry (TGA/MS) were employed due to their powerful ability for *in situ* analyzing the pyrolysis products from degradation. These investigations would surely help us to further understand the flame retardancy mechanism of the PC nanocomposite.

2. Experimental

2.1. Materials

Bisphenol A polycarbonate (Makrolon 2805) was purchased from Bayer (Shanghai), and solid bisphenol A bis(diphenyl phosphate) (S-BDP) was provided by Yoke Chemical Co., Ltd. The organo-montmorillonite (OMMT) was Nanomer I.44P from Nanocor Inc., which was cation-exchanged modified by dimethyl dihydrogenated tallow ammonium. PC and OMMT were dried for 12 h at 100 °C prior to process, whereas S-BDP was used as received.

2.2. Sample preparation

Dehumidified PC was melt blended with addictives by a co-rotating twin-screw extrusion procedure. The screw temperature profile was 235, 240, 245, 250, 242, 232 °C from the hopper to the die, and the rotary speed was 200 rpm. Subsequently, the extrudate was cooled in a water bath before being pelletized. The specimens for cone calorimetry were prepared by injection molding with an injection temperature profile of 250, 256, 263, 270, 265 °C from the hopper to the nozzle.

2.3. Characterizations

2.3.1. Transmission electron microscopy

The sample containing OMMT was cryo-microtomed with a glass knife under liquid nitrogen on a Leica ultracut UCT microtome, to give sections with a nominal thickness of 50 nm. The sections were then transferred to 200-mesh copper grids. Bright field transmission electron microscopy (TEM) images were obtained on a Hitachi H-800 at an accelerating voltage of 200 kV.

2.3.2. Cone calorimetry

Cone calorimeter measurements were performed at an incident radiant flux of 50 kW/m^2, according to ISO 5660 protocol, using a Fire Testing Technology apparatus with a truncated cone-shaped radiator. The specimen ($100 \times 100 \times 3$ mm^3) was measured horizontally without any grids. Parameters such as time to ignition (t_{ign}), heat release rate (HRR), maximum peak HRR (PHRR), time to PHRR (t_{PHRR}), total heat released (THR), remaining residue, average mass loss rate (AMLR), average effective heat of combustion (AEHC), average specific extinction area (ASEA), average carbon monoxide yield (ACOY) and average carbon dioxide yield (ACO_2Y) are recorded within the time of 700 s after tests started. These typical results from cone calorimeter were reproducible within ±10%, and the reported results are the average of three measurements.

2.3.3. TGA/FTIR

TGA/FTIR measurement was carried out on a Netzsch TG 209 F1 thermogravimeter coupled with a Nicolet 6700 FTIR spectrophotometer. About 10 mg of each sample was heated from 40 °C to 800 °C with a heating rate of 20 °C/min under nitrogen (flow rate = 60 ml/min). The couple system between TGA and FTIR was a quartz capillary kept at temperature of 200 °C.

2.3.4. TGA/MS

TGA/MS characterization was performed on a Netzsch STA 449 C-QMS 403 C instrument. TGA was performed in high purity argon at a flow rate of 25 ml/min. In the experiment, a sample weighing approximately 10 mg was heated also at 20 °C/min from 40 °C to 800 °C. Mass analysis was carried out using a spectrometer with an electron-impact ion source (70 eV); energy scanning was carried out in the range m/z 10–110 at a rate of 0.2 s^{-1} for each mass unit. The connection between TGA and MS was done by means of a quartz capillary at 200 °C as well.

3. Results and discussion

3.1. Dispersion of OMMT

According to our previous study [32], we chose three samples for investigations in this work (listed in Table 1).

Table 1
Compositions of the formulations.

Samples	PC[a] (%)	S-BDP[a] (%)	OMMT[a] (%)
PC	100	0	0
PC/S-BDP	92	8	0
PC/S-BDP/OMMT	92	6	2

[a] All the compositions of the formulations presented in this paper are described in terms of weight fraction.

Polytetrafluoroethylene (PTFE) was added as an anti-dripping agent to help the samples reach V-0 rating in the UL-94 burning tests. Since the TGA/FTIR and TGA/MS tests were scheduled herein, the composition of the samples in this research should preferably be as simple as possible. Thus, PTFE was excluded as can be seen from Table 1.

With absence of PTFE, dispersion of OMMT in the PC/S-BDP/OMMT sample was confirmed by TEM observation (Fig. 1). From the low magnification image, it can be seen that OMMT is uniformly distributed in the matrix. Swollen clay tactoids and single or a few layered clay platelets can be found in the high magnification image, suggesting a mainly intercalated and partially exfoliated morphology of the nanocomposite. There is not much difference compared with the OMMT dispersion observed in the previous study [32].

3.2. Cone calorimetry

Flame retardancy properties of S-BDP and OMMT in PC were quantitatively evaluated by cone calorimeter. Cone calorimeter is an effective bench scale apparatus to simulate real fire scenarios. Detailed data from cone calorimeter are reported in Fig. 2 and 3 and Table 2.

As can be seen in Fig. 2, the HRR curve of neat PC exhibits a sharp peak with a small shoulder ahead. This shape of the curve can be explained by the combustion behavior of the sample. Under the radiation of a 50 kW/m^2 heat flux, the surface of neat PC melts and

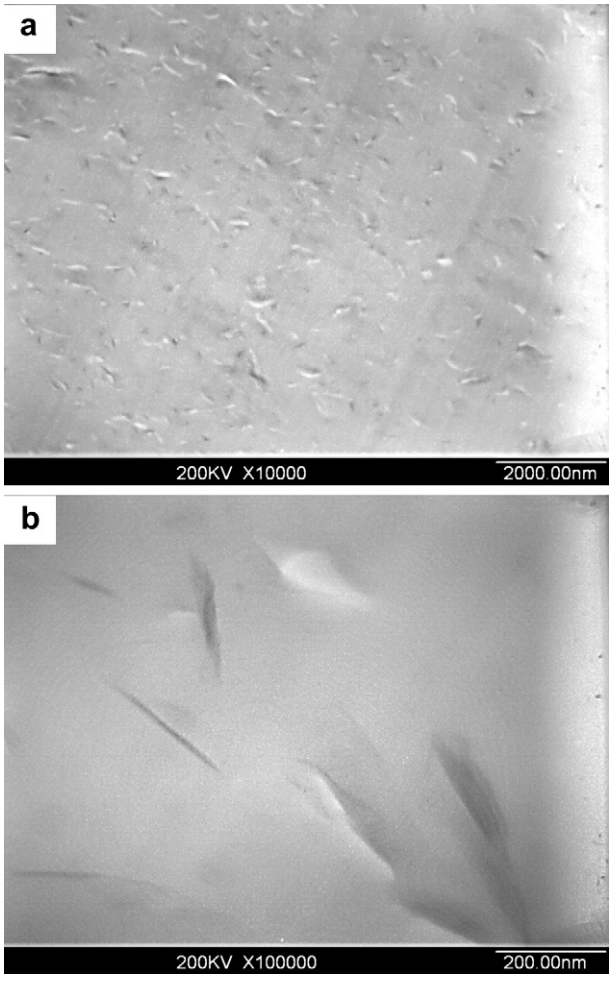

Fig. 1. TEM images of PC/S-BDP/OMMT: (a) low magnification; (b) high magnification.

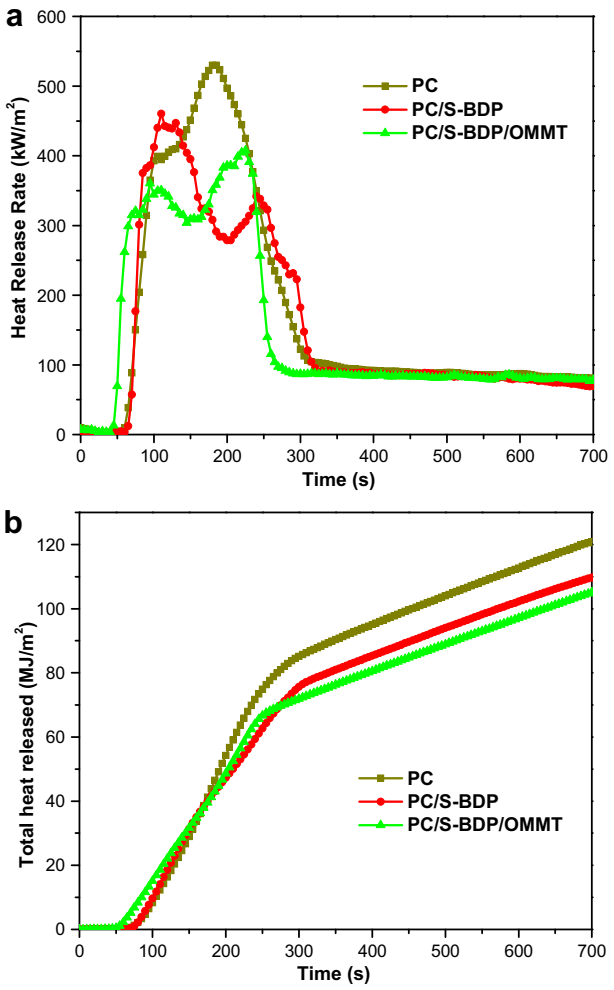

Fig. 2. (a) HRR and (b) THR curves of PC, PC/S-BDP and PC/S-BDP/OMMT.

then forms a thin layer of char. The charred surface remains intact for a short period of time which corresponds to the appearance of the small shoulder. Subsequently, the charred surface is destroyed by the vigorous gas evolution of the underlying sample. As more flammable gases evolve to the air, the specimen burns more intensively to reach the PHRR of 528 kW/m^2. Char formation never stops during the whole time of burning. When most of the sample has been burnt out, which is after about 300 s as seen in the HRR curve, the leaving char residue remains slow glowing combustion so that the HRR maintains above zero until the testing stops.

S-BDP could promote char formation of PC during combustion. PC/S-BDP reaches its PHRR of 442 kW/m^2 at the beginning. Then the sample forms char more quickly and firmly to protect the underlying material so that the HRR decreases at the time of 130–240 s. After 240 s, the protecting shield breaks to exhibit another lower peak in the HRR curve. The first peak of HRR occurs earlier than neat PC, suggesting S-BDP could facilitate PC decomposition in the earlier stage.

When 2% S-BDP was substituted with OMMT, more amount of even compacter char residue could be formed. The HRR curve of PC/S-BDP/OMMT also exhibits two peaks as PC/S-BDP, only except that the higher peak is the second one. This is slightly different compared with adding S-BDP alone. It is postulated that OMMT could help to maintain the integrity of the layered char at earlier stage, the matrix would be better protected thus the first peak of HRR is not as intense as PC/S-BDP. However, the vigorous bubbling

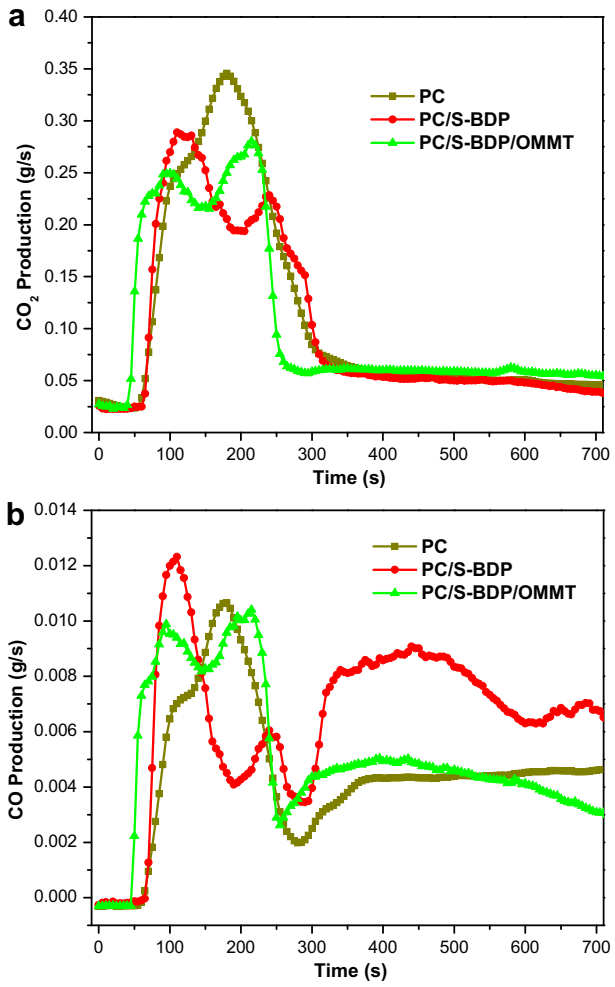

Fig. 3. (a) CO_2 and (b) CO production curves of PC, PC/S-BDP and PC/S-BDP/OMMT.

of the underneath matrix eventually burst the surface layered char. For there is more part of the matrix being protected in the earlier stage, it means there would be more parts of the matrix to burn in the later stage. This is why the second HRR peak of PC/S-BDP/OMMT is higher than PC/S-BDP. Here we see that the first HRR peak of PC/S-BDP/OMMT is also earlier than neat PC. However the t_{PHRR} is delayed compared with PC/S-BDP. Delayed t_{PHRR} is favorable, as it implies there would be more time for escaping during a real fire accident. Although the PHRR and THR are further reduced to 404 kW/m^2 and 105 MJ/m^2, respectively, the reduction is rather small compared to other polymer nanocomposites [38–42]. It should be also noted that the t_{ign} is drastically decreased as many other nanocomposites reported before [38–42].

Table 2
Some detailed cone calorimetric data.

	PC	PC/S-BDP	PC/S-BDP/OMMT
t_{ign} (s)	62 ± 3	63 ± 5	38 ± 5
PHRR (kW/m^2)	528 ± 31	442 ± 20	404 ± 13
t_{PHRR} (s)	183 ± 3	114 ± 2	228 ± 5
THR (MJ/m^2)	121 ± 3	110 ± 2	105 ± 2
Residue (%)	23 ± 1	29 ± 2	33 ± 1
AMLR (g/s)	0.049 ± 0.001	0.045 ± 0.0001	0.043 ± 0.001
AEHC (MJ/kg)	33.4 ± 0.5	34.5 ± 0.4	35.6 ± 0.3
ASEA (m^2/kg)	737 ± 12	786 ± 10	937 ± 5
ACOY (kg/kg)	0.11 ± 0.01	0.17 ± 0.02	0.13 ± 0.01
ACO_2Y (kg/kg)	2.30 ± 0.07	2.51 ± 0.05	2.52 ± 0.08

Effective heat of combustion is defined as the heat released per unit mass of material being volatilized during combustion. It can be presented as

$$EHC = \frac{HRR}{MLR}$$

where HRR is the heat release rate and MLR is the mass loss rate [43]. If a flame retardant exhibits flame inhibition in the gaseous phase, combustion of the volatilized materials would become incomplete and reduce the HRR to further show a reduced EHC. On the contrary, an increased EHC indicates the flame retardant exhibits a condensed phase effect.

It is acknowledged that BDP exhibits condensed phase effect as well as gaseous phase effect [4–6]. From Table 2, it can be seen that the amounts of residue and AEHC of PC/S-BDP and PC/S-BDP/OMMT are all elevated whereas AMLR are all reduced than those of neat PC, thus the flame retardant effects of S-BDP and OMMT mainly exist in the condensed phase. It's also noted that the AEHC of PC/S-BDP is slightly lower than that of PC/S-BDP/OMMT. It is assumed because of two reasons. One is that PC/S-BDP possesses 2% more S-BDP than PC/S-BDP/OMMT, the other is that S-BDP alone could present a little stronger gaseous phase effect of flame retardancy while combined with OMMT the condensed phase effect of S-BDP would be enhanced. This result would be further understood by the analysis of the pyrolysis products from thermal decomposition.

As for the smoke generated during combustion, unfortunately the ASEA, ACOY and ACO_2Y of PC/S-BDP and PC/S-BDP/OMMT are all increased compared to neat PC. Especially, the amount of carbon monoxide released is drastically enhanced when S-BDP is added alone due to the flame inhibition effect. Carbon monoxide is considered to be a fatal toxic gas in fire accidents. Although the ASEA of PC/S-BDP/OMMT is increased, the ACOY is decreased compared with PC/S-BDP. All these data implies that compared to S-BDP added alone, S-BDP combined with OMMT would cause severe light extinction but more importantly reduce the toxicity of the smoke.

From Fig. 3b, it can be observed that CO production is prominently reduced especially after 300 s which corresponds to the period of steady and slow combustion of the char residue. OMMT would migrate toward the surface of the matrix to exhibit an excellent barrier effect [44]. It is supposed that the hindered thermal transfer caused by the barrier effect can result an excess of heat upon the char surface, and consequently induce the char surface to be in a "hotter" state. When evolving through the surface, CO has to travel alone tortuous paths due to the barrier effect of OMMT; therefore CO could have more retention time with the "hotter" surface with good chance of being further oxidized to be CO_2.

3.3. TGA

TGA curves and their corresponding DTG curves of all the formulations, derived from TGA/FTIR measurements, are shown in Fig. 4. The onset degradation temperatures (T_{onset}) are defined by the temperatures of 5% weight loss in TGA curves, whereas the maximum degradation temperatures (T_{max}) are evaluated by the peaks in DTG curves. Above detailed TGA and DTG data are listed in Table 3.

It can be seen from Fig. 4, neat PC exhibits only one degradation step in inert atmosphere during 450–600 °C. As an engineering plastic, PC has an outstanding thermal stability, for it starts to degrade at as high as 478 °C and the maximum weight loss rate occurs at 528 °C.

However, S-BDP and OMMT are not as stable as PC upon heat. Although the sample of PC/S-BDP begins to degrade a bit earlier at

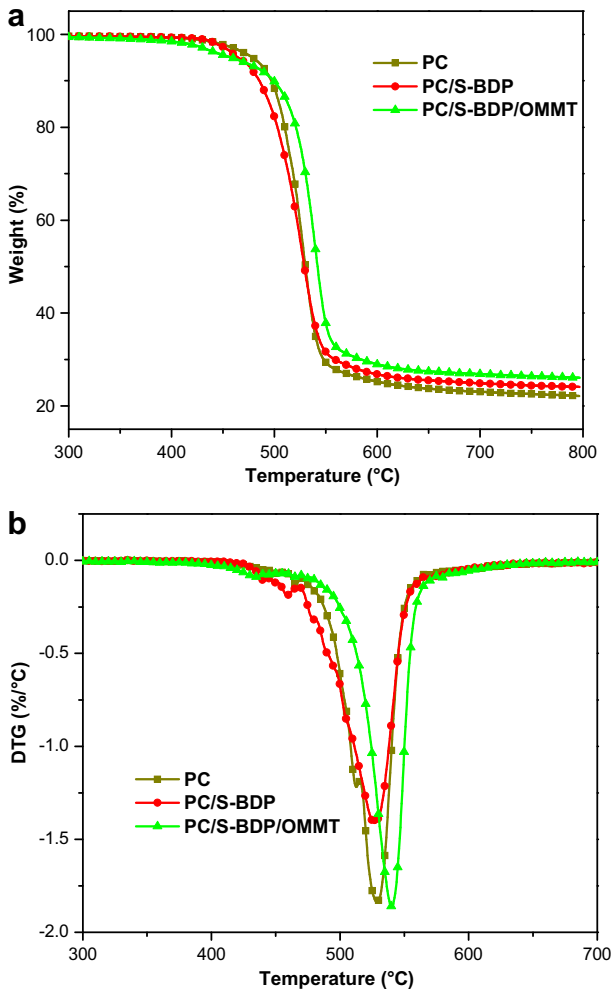

Fig. 4. (a) TGA and (b) DTG curves of PC, PC/S-BDP and PC/S-BDP/OMMT derived from TGA/FTIR measurements.

465 °C, the maximum weight loss rate shows at 527 °C, which is almost the same as neat PC. The result agrees with the combustion behavior in the cone calorimeter. S-BDP could facilitate PC decomposition in the earlier stage thus PC/S-BDP exhibits a lower T_{onset}; nevertheless, S-BDP could promote char formation of PC thereby decelerate further degradation and cause PC/S-BDP to have a same T_{max} as neat PC. Same phenomenon may be detected more obviously from the sample of PC/S-BDP/OMMT. PC/S-BDP/OMMT exhibits an even lower T_{onset} of 458 °C, but a drastically higher T_{max} of 539 °C. Poor thermal stability of ammonium surfactant used in organic modification of montmorillonite and decomposition of the matrix catalyzed by OMMT would contribute to the even lower T_{onset} [45]; however barrier effect of OMMT could cause PC/S-BDP/OMMT to show an even higher T_{max} than both neat PC and PC/S-BDP. Both char residues of PC/S-BDP and PC/S-BDP/OMMT at 800 °C are elevated compared with neat PC.

Table 3
TGA and DTG data derived from TGA/FTIR measurements.

Samples	T_{onset} (°C)	T_{max} (°C)	Char residue (%) at 800 °C
PC	478 ± 1	528 ± 1	22 ± 1
PC/S-BDP	465 ± 2	527 ± 1	24 ± 1
PC/S-BDP/OMMT	458 ± 2	539 ± 1	26 ± 1

3.4. TGA/FTIR

Evolved gases from TGA furnace were inspected by FTIR simultaneously. Fig. 5 shows the 3D FTIR spectra of gaseous products of all the formulations during thermal degradation. It can be noted that the most intensive absorbance band in all the three spectra is around 2360 cm^{-1}, which is the main product, carbon dioxide (CO_2), evolved from degradation of PC. Moreover, all the three formulations exhibit virtually one infrared absorbing period of time. Other than above, no more information can be easily detected from the 3D FTIR spectra.

FTIR spectra were obtained repeatedly over time during TGA/FTIR measurement, and a Gram–Schmidt reconstruction curve can be plotted based on all the individual spectra. Every point of the Gram–Schmidt curve is calculated by the infrared extinction coefficient of the evolved gases and their corresponding concentrations. In another word, the Gram–Schmidt curve should indicate the total FTIR absorbance intensity of all the evolved gaseous components over the entire tested wavenumber range (4000–700 cm^{-1}) in each

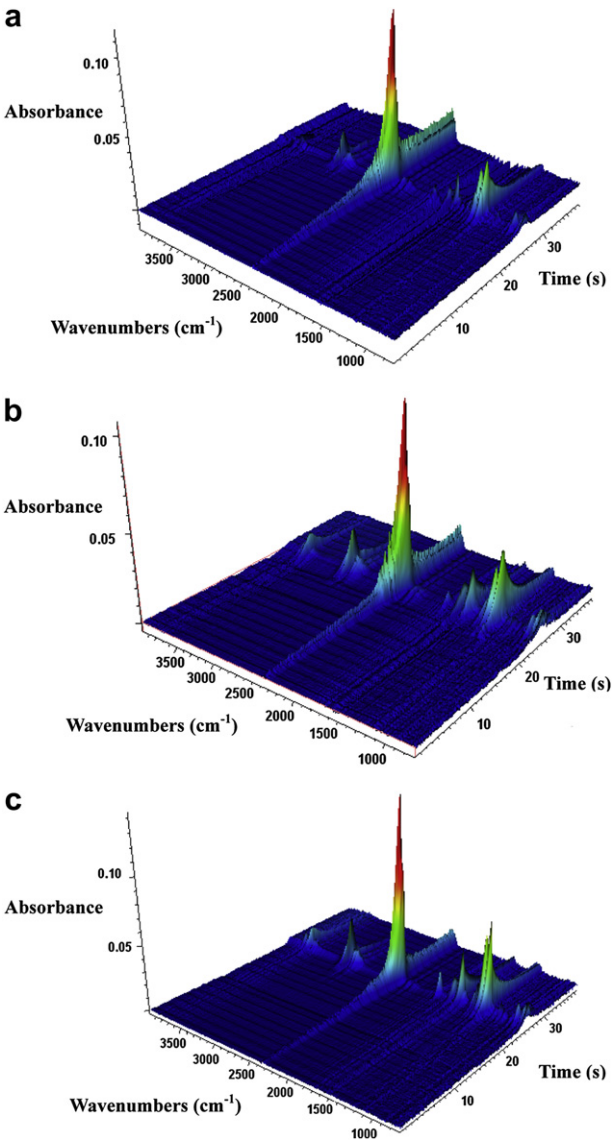

Fig. 5. 3D FTIR diagrams of gases evolved from thermal degradation of (a) PC, (b) PC/S-BDP and (c) PC/S-BDP/OMMT.

weight loss [46]. Gram–Schmidt curves of all the samples are presented in Fig. 6. As can be seen, all the Gram–Schmidt curves exhibit approximate one sharp peak which corresponds to the maximum weight loss in TGA. The peaks of PC, PC/S-BDP and PC/S-BDP/OMMT are at 24.9, 25.0 and 25.6 min, respectively. The heating rate is 20 °C/min, thus these peaks can be corresponded to 538, 540 and 552 °C in the TGA furnace. It indicates that the vigorous decomposition process of PC/S-BDP/OMMT would be delayed compared to neat PC and PC/S-BDP. It should also be noted that these peaks must be related to the T_{max}s deduced from DTG curves; however, the peaks of Gram–Schmidt are all shifted to higher corresponding temperatures than the T_{max}s. The shift of the peaks may attribute to the delay time between the gas generation and its detection in the FTIR spectrometer, since all the pyrolysis components have to travel through the quartz capillary between the TGA and the FTIR equipments. Notwithstanding, the enhancement of temperature between the peaks of neat PC and PC/S-BDP/OMMT in the Gram–Schmidt curves approximately coincides with the increment of T_{max} in the corresponding DTG curves.

FTIR spectra of pyrolysis products of all the formulations at their maximum weight loss rates are presented in Fig. 7. The wavenumber range of 2750–1900 cm^{-1} is skipped in the figure. Assignments of some main absorbance bands in the spectra are summarized in Table 4. It is believed that alcoholysis or hydrolysis of carbonate linkage is one of the main degradation pathways of PC, thus free phenol derivatives can be identified by the absorbance bands of 3650 cm^{-1} from –OH vibration, 1605 and 1510 cm^{-1} from C–C stretching and skeletal vibration of aromatic rings, 1240 and 1190 cm^{-1} from C–O vibration, as well as 830 and 750 cm^{-1} from C–H deformation vibration of aromatic rings [36,47,48]. Besides, the isopropylidene linkage would eliminate methyl to form methane, supported by the absorbance bands at 3015 and 1305 cm^{-1} from C–H stretching and deformation vibrations of methane, respectively.

It also should be noted that the substituted types of the aromatic components can be discerned by FTIR characterization. The peak at 830 cm^{-1} is the distinctive absorbance band of *para* disubstituted aromatic compounds, whereas the peak at 750 cm^{-1} is the typical absorbance band of monosubstituted and/or *ortho* disubstituted aromatic compounds [36,48]. The existence of *ortho* disubstituted aromatic fragments may confirm the Fries rearrangement reaction of carbonate in the polymer chains (Fig. 8).

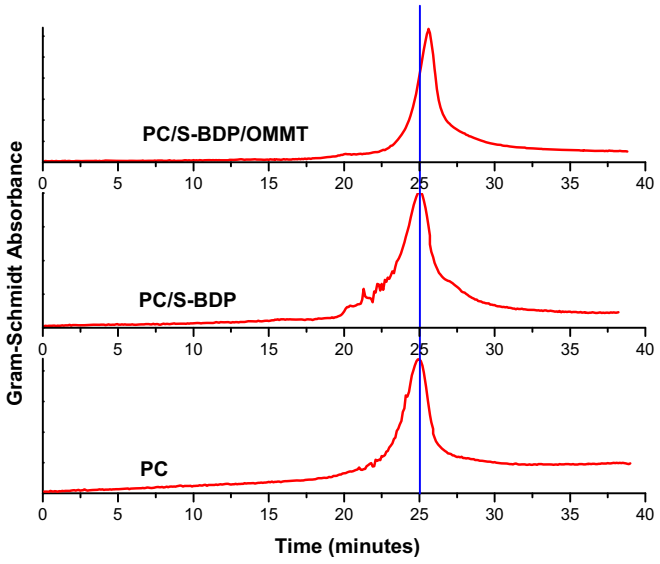

Fig. 6. Gram–Schmidt curves of PC, PC/S-BDP and PC/S-BDP/OMMT.

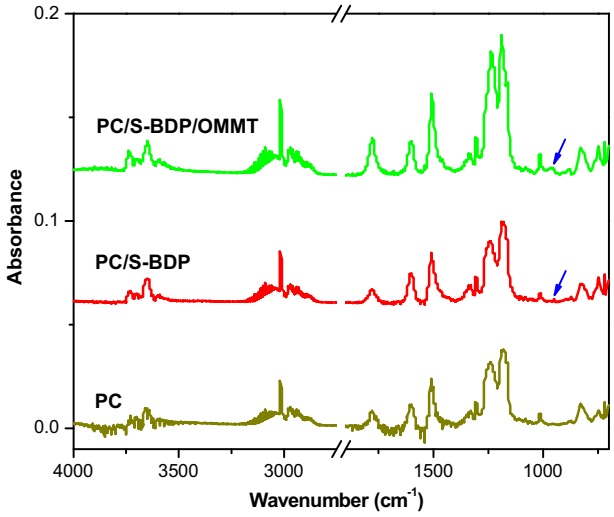

Fig. 7. FTIR spectra of pyrolysis products of PC, PC/S-BDP and PC/S-BDP/OMMT at their maximum weight loss rates.

PC/S-BDP and PC/S-BDP/OMMT exhibit almost the same absorbance bands compared with neat PC, except for the very weak absorbance at 960 cm^{-1} which can be assigned to P–O–C stretching vibration [49]. The absorbance is so negligible that it can be barely detected. This is due to the reason that S-BDP react with PC mainly in the condensed phase as well as slightly in the gaseous phase during thermal degradation, a very large amount of phosphorus-containing components may be kept in the char residues other than evolving to the gaseous phase.

Furthermore, there is a quantitative difference among the absorbance bands in the spectra of PC/S-BDP/OMMT compared with neat PC and PC/S-BDP. The intensity ratio of the carbonyl absorbance band of carbonate (1778 cm^{-1}) to its nearby band (1605 cm^{-1}, aromatic rings vibration absorbance) in the spectra of PC/S-BDP/OMMT is a little higher than that in the spectra of neat PC and PC/S-BDP. It indicates that more carbonate linkage structures are preserved in PC/S-BDP/OMMT. Jang et al. previously found that phosphate may stabilize carbonate linkage from oxidative degradation in air atmosphere TGA [49]. However in our observation, S-BDP alone couldn't stabilize carbonate linkage evidently during thermal degradation under the inert atmosphere. More carbonate linkage could be preserved only when OMMT is added. It's worthy to be noted that carbonate linkage is a rather crucial reagent for char formation through Fries rearrangement reaction and other reactions with phosphates [4,32,36]. Therefore, more preserved carbonate linkage is beneficial for enhancing the flame retardancy of PC.

Table 4
Assignment of some main absorbance bands in the FTIR spectra.

Wavenumber (cm^{-1})	Assignment
3740–3600	O–H stretching vibration of phenol or water
3160–3057	C–H stretching vibration of aromatic rings
3015, 1305	C–H stretching and deformation vibration of methane
2970–2885	C–H stretching vibration of $-CH_3$ and $-CH_2-$
17780	C=O stretching vibration of carbonate
1605, 1510	Ring stretching and skeletal vibration of aromatic rings
1342, 1332	C–H deformation vibration of isopropylidene group
1240, 1190	C–O stretching vibration of aromatic ether
960	P–O–C stretching vibration
830, 750	C–H deformation vibration of aromatic rings

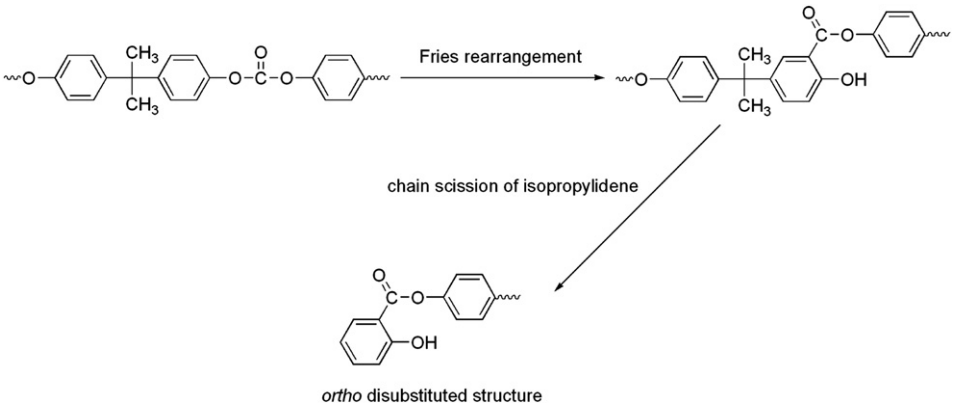

Fig. 8. Fries rearrangement reaction of carbonate in the polymer chains.

It has been demonstrated that montmorillonite could somewhat alter the degradation pathways of polystyrene [41,50,51], polyamide 6 [39] and poly(styrene-*co*-acrylonitrile) [40]. However, from the discussion above, it seems that the OMMT used in this paper would not greatly change the degradation pathways of the matrix. It might explain why OMMT provide a relatively smaller reduction of PHRR in PC than other polymer matrices as showed above in the cone calorimeter tests. Regarding the reduced CO production of S-BDP combined with OMMT observed the cone calorimetry, unfortunately it cannot be found in the TGA/FTIR or the following TGA/MS tests, since the samples were burned under participation of oxygen in the former test whereas an inert atmosphere in the latter two tests.

3.5. TGA/MS

FTIR measurement investigates only the functional group information about the pyrolysis products, exact composition of the pyrolysis products can be established by mass spectroscopy. Detailed results obtained from TGA/MS characterizations are

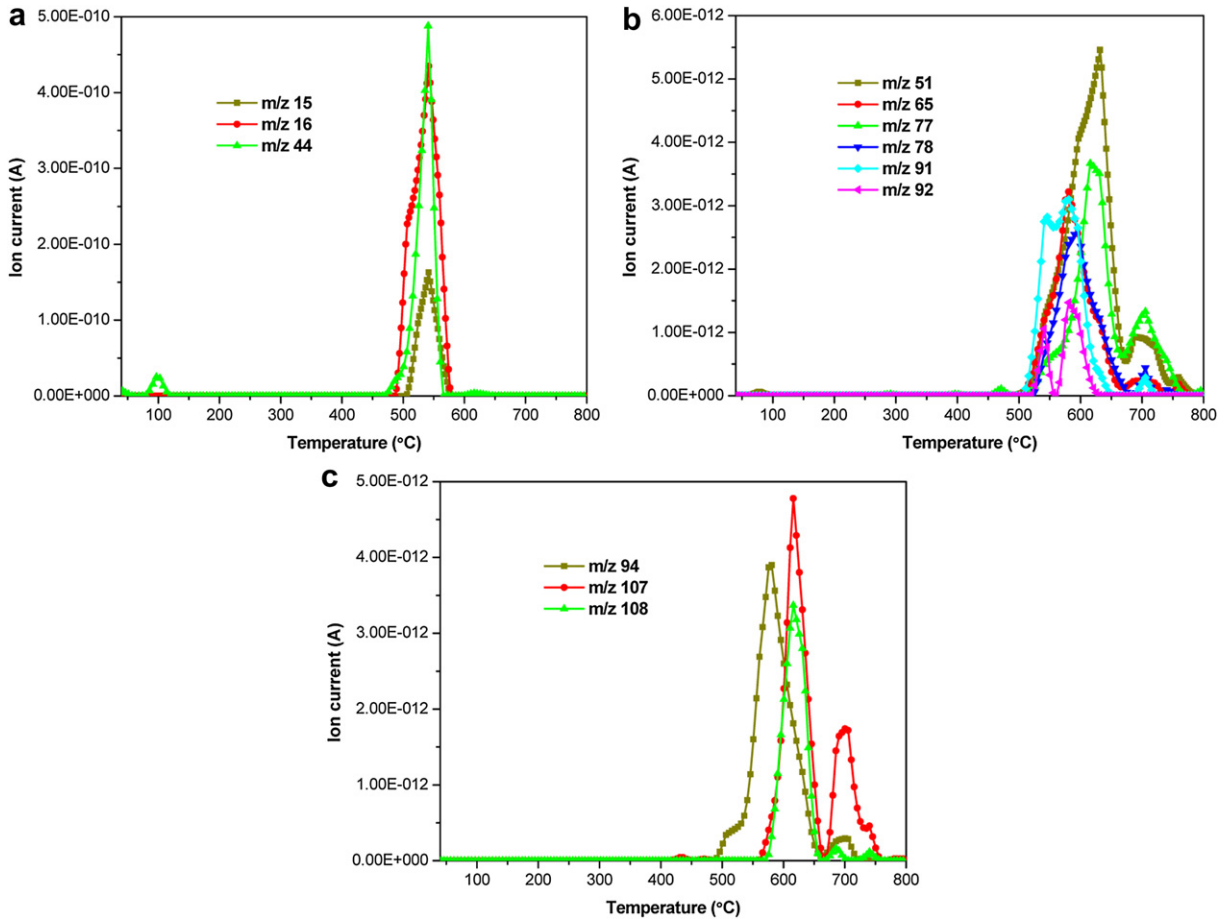

Fig. 9. Single ion current curves for the fragments generated from thermal degradation of neat PC: (a) $m/z = 15, 16, 44$; (b) $m/z = 51, 65, 77, 78, 91, 92$; and (c) $m/z = 94, 107, 108$.

presented in the form of single ion current curves for the pyrolysis species produced from degradation of neat PC, PC/S-BDP and PC/S-BDP/OMMT, shown in Fig. 9–11, respectively.

It can be observed from Fig. 9 that intensive signals of the species with different ratios of mass to charge (m/z) appear within the temperature range of 500–650 °C. This temperature range is also a little higher than that of the degradation stage described in the TGA measurement due to the delay time between sample degradation and mass spectroscopy. Carbon dioxide can be determined by the m/z 44, and methane can be confirmed by the m/z 15 and 16. Fragments of m/z 78 and 92 belong to benzene and toluene with additional evidence of diagnostic fragments of aromatic rings of m/z 51, 65, 77 and 91. Phenol (m/z 94) and methyl phenol (m/z 107, 108) can be also identified. These data above firmly support the results from TGA/FTIR. However, species with carbonate linkage could be barely detected in MS investigation. It's assumed that carbonate linkage would be easily destroyed to generate CO_2 during the electron-impact ionization.

PC/S-BDP and PC/S-BDP/OMMT exhibit somewhat alike results as neat PC. Methane, CO_2, benzene, toluene, phenol and methyl phenol are all perceived. Nevertheless, there are still some new fragments which are detected from degradation of both PC/S-BDP and PC/S-BDP/OMMT. The signals of m/z 47 and 63 (Figs. 10d and 11d) can be assigned to $OP^{+}\bullet$ and O_2P^{+} produced from degradation of phosphates [52]. Define

$$R = \frac{I(47)_{max}}{I(63)_{max}}$$

where $I(47)_{max}$ and $I(63)_{max}$ are the maximum ion currents of the species of m/z 47 and 63, respectively. The R for PC/S-BDP is 1.11, whereas 0.98 for PC/S-BDP/OMMT. Since R is a relative calculation and not associated with the actual amount of S-BDP in each sample, thus it can conclude that PC/S-BDP could generate more PO radicals than PC/S-BDP/OMMT during thermal degradation. Besides, the PO radicals are the main effective species responsible for flame inhibition [53], it indicates that S-BDP alone would exhibit slightly stronger gaseous phase effect of flame retardancy than S-BDP combined with OMMT. In other words, the condensed phase effect of S-BDP would be enhanced with the presence of OMMT. This phenomenon is connected with the relatively delayed decomposition of PC/S-BDP/OMMT discussed in DTG and Gram–Schmidt curves previously. The barrier effect of OMMT would compel pyrolysis products to escape alone tortuous paths, thereby create more opportunities for pyrolysis products of S-BDP to react with those of the matrix. Consequently S-BDP could exhibit stronger effect in the condensed phase rather than the gaseous phase. Moreover, this phenomenon also confirms our previous assumption discussed in the cone calorimeter tests: despite the excess 2% S-BDP, stronger gaseous phase effect acted by S-BDP alone would contribute to the slight reduced AEHC of PC/S-BDP than that of PC/S-BDP/OMMT.

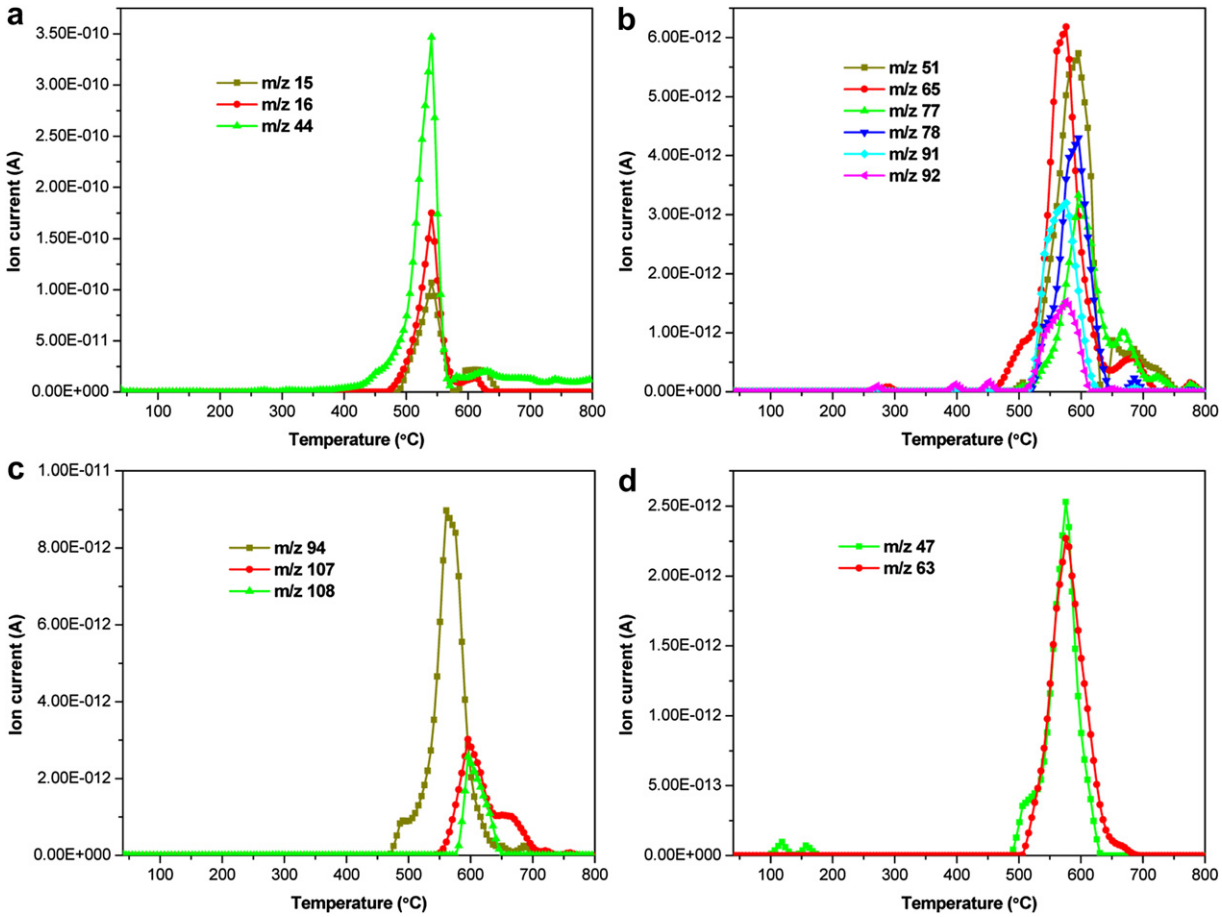

Fig. 10. Single ion current curves for the fragments generated from thermal degradation of PC/S-BDP: (a) $m/z = 15, 16, 44$; (b) $m/z = 51, 65, 77, 78, 91, 92$; (c) $m/z = 94, 107, 108$; and (d) $m/z = 47, 63$.

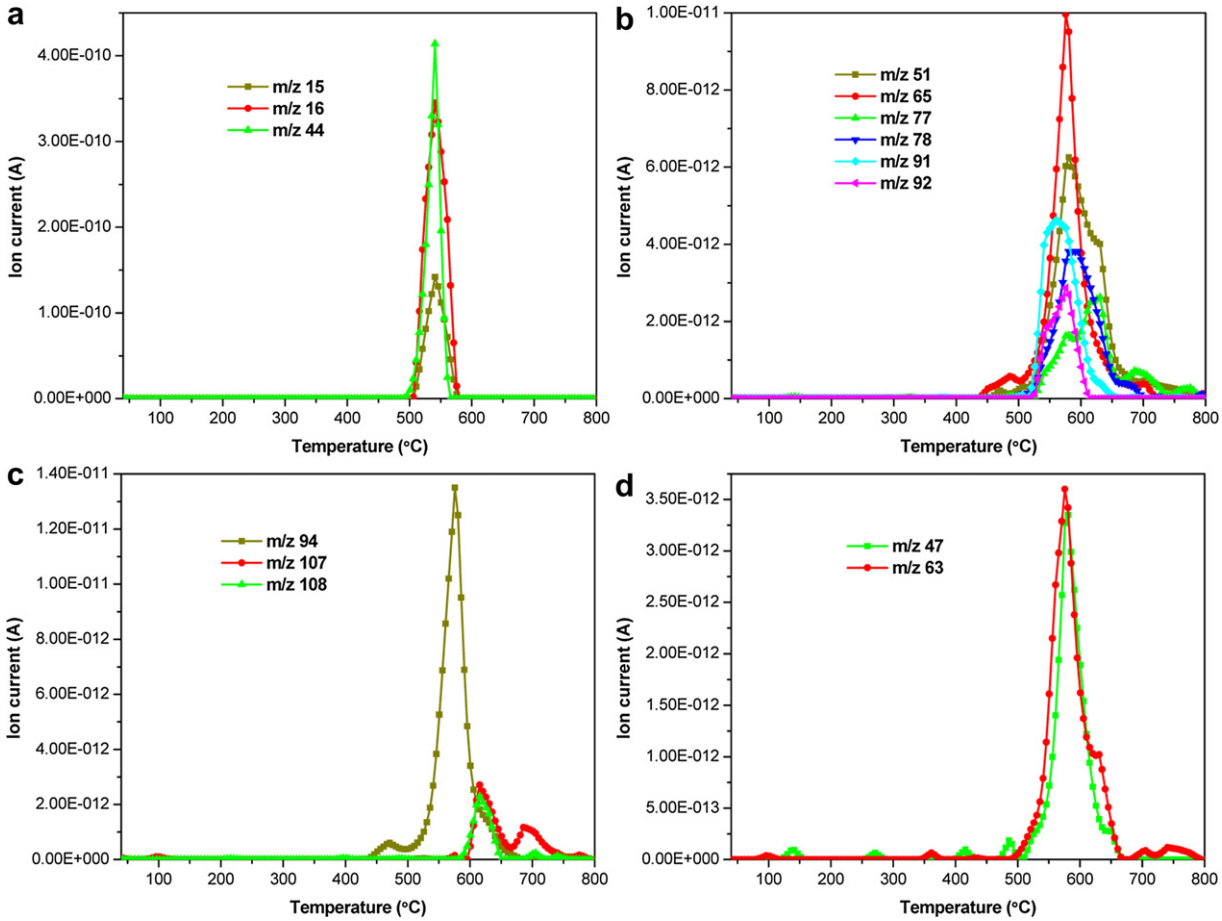

Fig. 11. Single ion current curves for the fragments generated from thermal degradation of PC/S-BDP/OMMT: (a) $m/z = 15, 16, 44$; (b) $m/z = 51, 65, 77, 78, 91, 92$; (c) $m/z = 94, 107, 108$; and (d) $m/z = 47, 63$.

4. Conclusions

Thermal degradation and flame retardancy mechanisms of polycarbonate filled with solid bisphenol A bis(diphenyl phosphate) and montmorillonite were comprehensively cross-examined by cone calorimetry, TGA/FTIR and TGA/MS.

Firstly the polycarbonate nanocomposite morphology was confirmed with TEM to be mainly intercalated and partially exfoliated. Under an inert atmosphere, the main pyrolysis products evolved from thermal degradation of polycarbonate are carbon dioxide, methane, carbonates, benzene and its derivatives, as well as phenol and its derivatives. These degradation products remain almost unchanged after the addition of S-BDP and OMMT. Nevertheless, the carbonate linkage could be stabilized by S-BDP combined with OMMT as revealed by TGA/FTIR. Eventually, vigorous decomposition process at higher temperature would be delayed and char residue formation would be promoted by the combination of S-BDP and OMMT fillers in PC. The flame retardancy effects of S-BDP and OMMT mainly exist in the condensed phase. Besides, S-BDP also exhibits slight effect in the gaseous phase, as revealed by the detection of phosphorus–oxygen radicals in TGA/MS. When S-BDP alone added in PC, the relative amount of PO was higher than that of S-BDP combined with OMMT. Thus, S-BDP added alone shows slightly stronger gaseous phase effect than the combination of S-BDP and OMMT. The enhanced condensed phase effect of S-BDP under the presence of OMMT is attributed to the barrier effect of OMMT. Due to the reason that the degradation pathways of polycarbonate wouldn't be greatly affected by S-BDP and OMMT, the values of PHRR obtained from cone calorimeter is not effectively reduced. Yet the fire behavior of polycarbonate during combustion could be changed by S-BDP and OMMT, especially the time to PHRR is largely delayed by S-BDP combined with OMMT. Furthermore, the OMMT could beneficially suppress the CO production probably by further oxidation of CO due to the barrier effect of OMMT.

The disclosed correlation between thermal degradation and flame retardancy mechanism may offer the potential of tailoring of the material in the future.

Acknowledgment

This work was sponsored by the National High Technology Research and Development Program of China ("863" Program) (No. 2007AA03Z538). Also the authors would like to express great appreciations to Mr. Hongqiang Qu from Heibei University, for the testing and fruitful discussion of TGA/MS.

References

[1] Innes J, Innes A. Flame retardants for polycarbonate – new and classical solutions. Plast Addit Compd 2006;8:26–9.
[2] Levchik SV, Weil ED. Overview of recent developments in the flame retardancy of polycarbonates. Polym Int 2005;54:981–98.
[3] Levchik SV, Weil ED. Flame retardants in commercial use or in advanced development in polycarbonates and polycarbonate blends. J Fire Sci 2006;24:137–51.
[4] Pawlowski KH, Schartel B. Flame retardancy mechanisms of triphenyl phosphate, resorcinol bis(diphenyl phosphate) and bisphenol bis(diphenyl

phosphate) in polycarbonate/acrylonitrile-butadiene-styrene blends. Polym Int 2007;56:1404–14.
[5] Perret B, Pawlowski KH, Schartel B. Fire retardancy mechanisms of aryl-phosphates in polycarbonate (PC) and PC/acrylonitrile-butadiene-styrene. J Therm Anal Calorim 2009;97:949–58.
[6] Pawlowski KH, Schartel B, Fichera MA, Jager C. Flame retardancy mechanisms of bisphenol A bis(diphenyl phosphate) in combination with zinc borate in bisphenol A polycarbonate/acrylonitrile-butadiene-styrene blends. Thermochim Acta 2010;498:92–9.
[7] Okada A, Usuki A. Twenty years of polymer-clay nanocomposites. Macromol Mater Eng 2006;291:1449–76.
[8] Tjong SC. Structural and mechanical properties of polymer nanocomposites. Mater Sci Eng R 2006;53:73–197.
[9] Chen B, Evans JRG, Greenwell HC, Boulet P, Coveney PV, Bowden AA, et al. A critical appraisal of polymer-clay nanocomposites. Chem Soc Rev 2008;37:568–94.
[10] Paul DR, Robeson LM. Polymer nanotechnology: nanocomposites. Polymer 2008;49:3187–204.
[11] Zou H, Wu SS, Shen J. Polymer/silica nanocomposites: preparation, characterization, properties, and applications. Chem Rev 2008;108:3893–957.
[12] Kumar AP, Depan D, Tomer NS, Singh RP. Nanoscale particles for polymer degradation and stabilization—trends and future perspectives. Prog Polym Sci 2009;34:479–515.
[13] Potschke P, Bhattacharyya AR, Janke A. Carbon nanotube-filled polycarbonate composites produced by melt mixing and their use in blends with polyethylene. Carbon 2004;42:965–9.
[14] Sung YT, Kum CK, Lee HS, Byon NS, Yoon HG, Kim WN. Dynamic mechanical and morphological properties of polycarbonate/multi-walled carbon nanotube composites. Polymer 2005;46:5656–61.
[15] Jin SH, Choi DK, Lee DS. Electrical and rheological properties of polycarbonate/multiwalled carbon nanotube nanocomposites. Colloid Surf A 2008;313:242–5.
[16] Pegel S, Potschke P, Petzold G, Alig I, Dudkin SM, Lellinger D. Dispersion, agglomeration, and network formation of multiwalled carbon nanotubes in polycarbonate melts. Polymer 2008;49:974–84.
[17] Abbasi S, Carreau PJ, Derdouri A. Flow induced orientation of multiwalled carbon nanotubes in polycarbonate nanocomposites: rheology, conductivity and mechanical properties. Polymer 2010;51:922–35.
[18] Kim H, Macosko CW. Processing-property relationships of polycarbonate/graphene composites. Polymer 2009;50:3797–809.
[19] Yoon PJ, Hunter DL, Paul DR. Polycarbonate nanocomposites. Part 1. Effect of organoclay structure on morphology and properties. Polymer 2003;44:5323–39.
[20] Yoon PJ, Hunter DL, Paul DR. Polycarbonate nanocomposites. Part 2. Degradation and color formation. Polymer 2003;44:5341–54.
[21] Wu DF, Wu LF, Zhang M, Wu L. Effect of epoxy resin on rheology of polycarbonate/clay nanocomposites. Eur Polym J 2007;43:1635–44.
[22] Dong QX, Chen QJ, Yang W, Zheng YL, Liu X, Li YL, et al. Thermal properties and flame retardancy of polycarbonate/hydroxyapatite nanocomposite. J Appl Polym Sci 2008;109:659–63.
[23] Pawlowski KH, Schartel B. Flame retardancy mechanisms of aryl phosphates in combination with boehmite in bisphenol A polycarbonate/acrylonitrile-butadiene-styrene blends. Polym Degrad Stab 2008;93:657–67.
[24] Song L, He QL, Hu Y, Chen H, Liu L. Study on thermal degradation and combustion behaviors of PC/POSS hybrids. Polym Degrad Stab 2008;93:627–39.
[25] Sanchez-Soto M, Schiraldi DA, Illescas S. Study of the morphology and properties of melt-mixed polycarbonate-POSS nanocomposites. Eur Polym J 2009;45:341–52.
[26] Zhang W, Li X, Guo X, Yang R. Mechanical and thermal properties and flame retardancy of phosphorus-containing polyhedral oligomeric silsesquioxane (DOPO-POSS)/polycarbonate composites. Polym Degrad Stab 2010;95:2541–6.
[27] Wang ZB, Xie GW, Wang X, Li GC, Zhang ZK. Rheology enhancement of polycarbonate/calcium carbonate nanocomposites prepared by melt-compounding. Mater Lett 2006;60:1035–8.
[28] Carrion FJ, Sanes J, Bermudez MD. Influence of ZnO nanoparticle filler on the properties and wear resistance of polycarbonate. Wear 2007;262:1504–10.
[29] Valmikanathan OP, Stroverkhova O, Mulla IS, Vijayamohanan K, Atre SV. The effect of synthesis procedure on the structure and properties of palladium/polycarbonate nanocomposites. Polymer 2008;49:3413–8.
[30] Chigwada G, Wilkie CA. Synergy between conventional phosphorus fire retardants and organically-modified clays can lead to fire retardancy of styrenics. Polym Degrad Stab 2003;81:551–7.
[31] Pack S, Kashiwagi T, Cao CH, Korach CS, Lewin M, Rafailovich MH. Role of surface interactions in the synergizing polymer/clay flame retardant properties. Macromolecules 2010;43:5338–51.
[32] Feng J, Hao JW, Du JX, Yang RJ. Flame retardancy and thermal properties of solid bisphenol A bis(diphenyl phosphate) combined with montmorillonite in polycarbonate. Polym Degrad Stab 2010;95:2041–8.
[33] Puglisi C, Sturiale L, Montaudo G. Thermal decomposition processes in aromatic polycarbonates investigated by mass spectrometry. Macromolecules 1999;32:2194–203.
[34] Carroccio S, Puglisi C, Montaudo G. Mechanisms of thermal oxidation of poly(bisphenol A carbonate). Macromolecules 2002;35:4297–305.
[35] Montaudo G, Carroccio S, Puglisi C. Thermal oxidation of poly(bisphenol A carbonate) investigated by SEC/MALDI. Polym Degrad Stab 2002;77:137–46.
[36] Jang BN, Wilkie CA. A TGA/FTIR and mass spectral study on the thermal degradation of bisphenol A polycarbonate. Polym Degrad Stab 2004;86:419–30.
[37] Jang BN, Wilkie CA. The thermal degradation of bisphenol A polycarbonate in air. Thermochim Acta 2005;426:73–84.
[38] Jang BN, Costache M, Wilkie CA. The relationship between thermal degradation behaviour of polymer and the fire retardancy of polymer/clay nanocomposites. Polymer 2005;46:10678–87.
[39] Jang BN, Wilkie CA. The effect of clay on the thermal degradation of polyamide 6 in polyamide 6/clay nanocomposites. Polymer 2005;46:3264–74.
[40] Jang BN, Wilkie CA. The effects of clay on the thermal degradation behaviour of poly(styrene-co-acrylonitrile). Polymer 2005;46:9702–13.
[41] Jang BN, Wilkie CA. The thermal degradation of polystyrene nanocomposite. Polymer 2005;46:2933–42.
[42] Morgan AB. Flame retarded polymer layered silicate nanocomposites: a review of commercial and open literature systems. Polym Adv Technol 2006;17:206–17.
[43] ISO 5660-1. Reaction-to-fire tests — heat release, smoke production and mass loss rate — Part 1: Heat release rate (cone calorimeter method). ISO; 2000.
[44] Tang Y, Lewin M. New aspects of migration and flame retardancy in polymer nanocomposites. Polym Degrad Stab 2008;93:1986–95.
[45] Qin HL, Zhang SM, Zhao CG, Hu GJ, Yang MS. Flame retardant mechanism of polymer/clay nanocomposites based on polypropylene. Polymer 2005;46:8386–95.
[46] Awad WH, Wilkie CA. Investigation of the thermal degradation of polyurea: the effect of ammonium polyphosphate and expandable graphite. Polymer 2010;51:2277–85.
[47] Perret B, Schartel B. The effect of different impact modifiers in halogen-free flame retarded polycarbonate blends – I. Pyrolysis. Polym Degrad Stab 2009;94:2194–203.
[48] Song QX, Wang Y. Infrared Spectroscopy and Raman Spectroscopy. In: Zhang ZX, editor. Analysis of organic spectroscopy. Beijing: People's Medical Publishing House; 2009. p. 116–30.
[49] Jang BN, Wilkie CA. The effects of triphenylphosphate and recorcinolbis(diphenylphosphate) on the thermal degradation of polycarbonate in air. Thermochim Acta 2005;433:1–12.
[50] Chen K, Susner MA, Vyazovkin S. Effect of the brush structure on the degradation mechanism of polystyrene-clay nanocomposites. Macromol Rapid Commun 2005;26:690–5.
[51] Chen K, Vyazovkin S. Mechanistic differences in degradation of polystyrene and polystyrene-clay nanocomposite: thermal and thermo-oxidative degradation. Macromol Chem Phys 2006;207:587–95.
[52] Balabanovich AI, Pospiech D, Haussler L, Harnisch C, Doring M. Pyrolysis behaviour of phosphorus polyesters. J Anal Appl Pyrol 2009;86:99–107.
[53] Green J. Phosphorus-containing flame retardants. In: Grand AF, Wilkie AC, editors. Fire retardancy of polymeric materials. New York: Marcel Dekker; 2000. p. 148–50.